



Great Hammerhead (*Sphyrna mokarran*)

Supplementary Information for *Sphyrna mokarran*

Rigby, C.L., Dulvy, N.K., Carlson, J., Fernando, D., Fordham, S., Jabado, R.W., Liu, K.M., Marshall, A., Pacoureau, N., Romanov, E., Sherley, R.B. & Winker, H.

To analyse the *Sphyrna mokarran* population trend data, we used a Bayesian state-space tool for trend analysis of abundance indices for IUCN Red List assessment (Just Another Red List Assessment, JARA), which builds on the Bayesian state-space tool for averaging relative abundance indices by Winker *et al.* (2018). The relative abundance or the population follows an exponential state-space population model of the form: $\mu_{t+1} = \mu_t + r_t$, where μ_t is the logarithm of the expected abundance in year t , and r_t is the normally distributed annual rate of change with mean \bar{r} , the estimable mean rate of change for a population, and process variance σ^2 . We linked the logarithm of the observed relative abundance $I_{t,i}$ for index i (where multiple datasets were available for the same fishery or region) to the expected abundance trend $\log(\hat{I}_t) = \mu_t$ using the observation equation (eqn. 16) from Winker *et al.* (2018). We used a non-informative normal prior for $\bar{r} \sim N(0, 1000)$. Priors for the process variance can be either fixed or estimated (see Winker *et al.* 2018 for details). If estimated (default), the priors were $\sigma^2 \sim 1/\text{gamma}(0.01, 0.01)$, or approximately uniform on the log scale (e.g. Chaloupka and Balazs 2007). Three Monte Carlo Markov chains were run and initiated by assuming a prior distribution on the initial state centred around the first data point in each abundance time series ($y_{t=1}$), $\mu_1 \sim N(\log(y_1), 1000)$. The first 20,000 iterations were discarded as burn-in, and of the remaining 200,000 iterations, 100,000 were selected for posterior inference. Thus, posterior distributions were estimated from 300,000 iterations. Analyses were performed using the R Statistical Software v3.5.0 (R Core Team 2018), via the interface from R ('r2jags' library v 0.5-7; Su and Yajima 2015) to JAGS ('Just Another Gibbs Sampler' v4.3.0; Plummer 2003). Convergence was diagnosed using Geweke's diagnostic (Geweke 1992) with thresholds of $p = 0.05$, via the 'coda' library (v0.19-1; Plummer *et al.* 2006).

The percentage change $D\%$ was directly calculated from the posteriors of the estimated population time series \hat{I}_t . If the span of \hat{I}_t was longer than 3 x generation length (GL), the percentage change was automatically calculated as the difference between a three-year average around the final observed data point T , and a three-year average around the year corresponding to $T - (3 \times \text{GL})$. The year $T + 1$ is always projected to obtain a three-year average around T . We used a three-year average to reduce the influence of short-term fluctuation (Froese *et al.* 2017). If the span of \hat{I}_t was shorter than 3 x GL, JARA projected forward, by passing the number of desired future years without observations to the model, to attain an \hat{I}_t that spans 3 x GL + 2 years for the calculation of $D\%$. These projections (shown as red dashed lines in the figures below) were based on the posteriors of the estimated population reduction across all n years in the observed time series: $\bar{r} = \frac{1}{n} \sum_{t=1}^n r_t$. The projection gives similar results to extrapolating backwards to attain a 3 x GL period and produces a similar result for the $D\%$.

We analysed the time series for each region where data were available, to produce a) a model fit to the observed data (e.g. Figure 1A), b) an annual rate of change (λ) based on the observed data ($\lambda = \exp(\bar{r})$), expressed as a % in e.g. Figure 1B), c) if needed, projected values for each year necessary to extend the time-series to 3 x GL (e.g. Figure 1C), and d) the posterior distribution for the regional rate of change (%) over 3 x GL (e.g. Figure 1D). Because the posterior distribution comprises an estimated % population change over 3 x GL for each model iteration, these automatically map to the IUCN Red List categories. For example, under criterion A2, an iteration yielding a % population change of +55% would be assigned to the Least Concern category, while iterations giving -82% and -55% would be assigned to Critically Endangered and Endangered, respectively. By assigning the posterior decline from each iteration in this way, it was possible to determine the most likely IUCN Red List category for each region separately (Table 1).

We then assessed the species globally (e.g. Figure 4) by calculating the expected rate of change (%) using the posterior probabilities for each of the regional rates of change weighted by an area-based estimate of the size of each region as a proportion of the species' global distribution. The current distribution map was used to calculate areas (Ebert *et al.* 2013). For any region where the species is known to occur, we sub-sampled (without replacement) from the posterior probability distribution for the regional rate of population reduction according to the proportion of the total area of a species' distribution that fell within that region. Where a species is known to occur in a region, but no regional trend data were available, we sampled from a uniform distribution, $U(-100,0)$ with the sample size determined by the proportion of the total area of the species' distribution that is contained within those regions.

Table 1. *Sphyrna mokarran* – Population change (%) and posterior probabilities for changes falling within the IUCN Red List categories Least Concern (LC), Near Threatened (NT), Vulnerable (VU), Endangered (EN), and Critically Endangered (CR); the “likely status” based on criteria A2–4 is assigned based on the category containing the highest posterior probability, with the exception that VU is also selected where LC obtained the highest probability, but it is < 50%. All probabilistic statements are based on the rate of change over three generation lengths (GL) from projections within JARA. The Global change is based on weighting the regional posterior probabilities by the proportional area (PA) weighting (see text for detail).

Region	GL (years)	Data length (years)	PA weighting	Median change	LC	NT	VU	EN	CR	Likely Status
N. Atlantic 1 ¹	24.8	25	0.27	-29.1	43.0	7.8	18.7	26.8	3.8	VU
N. Atlantic 2 ²	24.8	24	0.27	+366	100	0	0	0	0	LC
S. Atlantic	No trend data		0.05	–	–	–	–	–	–	–
N. Pacific	No trend data		0.24	–	–	–	–	–	–	–
S. Pacific	No trend data		0.16	–	–	–	–	–	–	–
Indian ³	23.7	26	0.28	-99.3	0	0	0	0	100	CR
Global 1	–	–	–	-62.4	20.5	6.6	14.0	20.8	38.1	CR
Global 2	–	–	–	-50.9	36.0	4.5	9.1	13.5	36.9	CR

Data sources:

1. Jiao *et al.* 2011: Figure 4M2, page 2702;
2. J. Carlson unpubl. data;
3. Dudley & Simpfendorfer 2006: Figure 2, page 231.

North Atlantic 1: Stock Assessment (1981–2005), Northwest Atlantic and Gulf of Mexico, relative abundance (numbers of sharks) (Jiao *et al.* 2011)

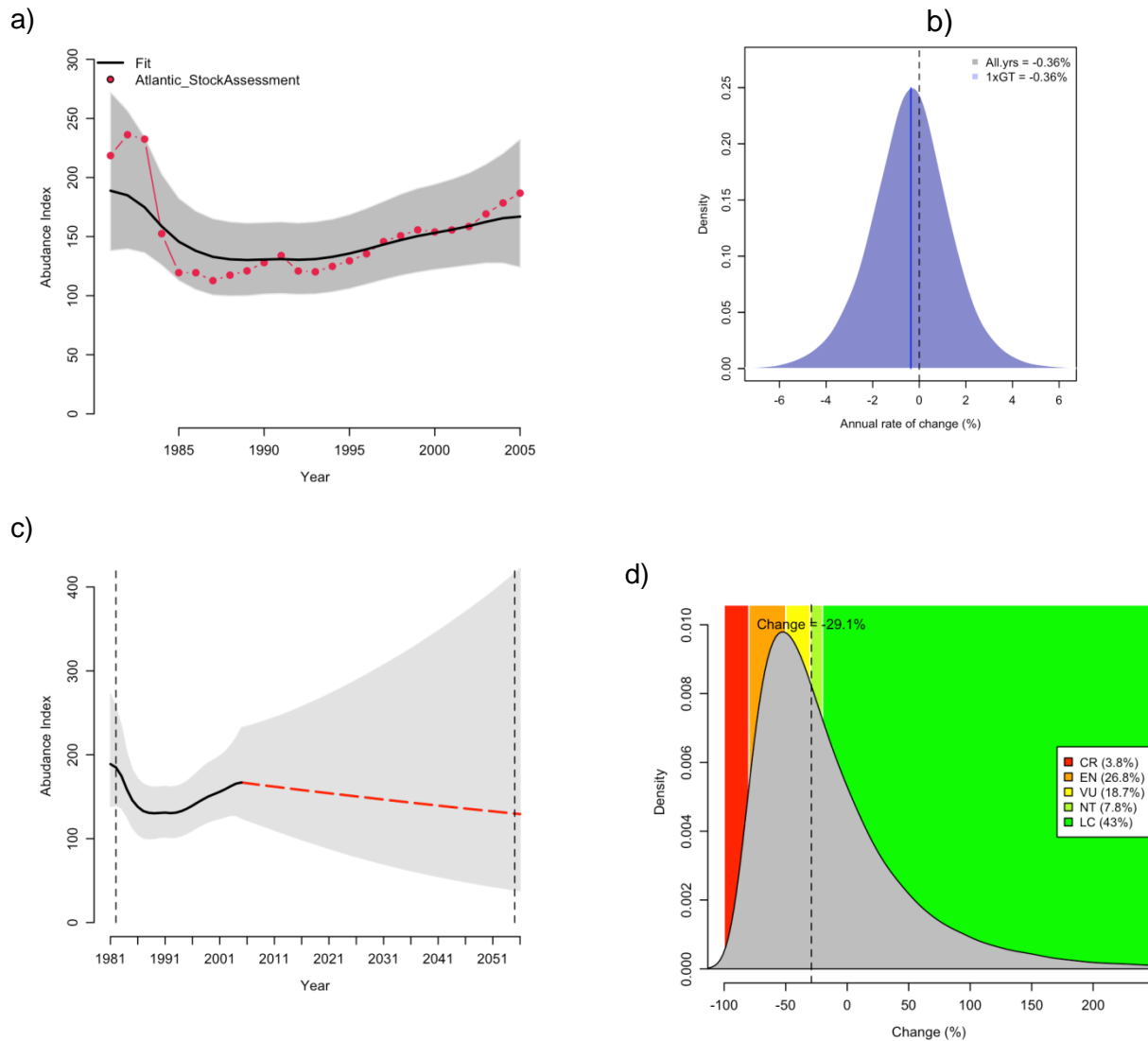


Figure 1. JARA results for Great Hammerhead (*Sphyrna mokarran*) in the north Atlantic showing (a) the JARA fit to the observed time-series, (b) the posterior probability for the percentage annual population change calculated from all the observed data (in black) and from the last 1 generation length (in blue), with the mean (solid lines) shown relative to a stable population (% change = 0, black dashed line), (c) the observed (black line) and predicted (red line) population trajectory over three generations (74.4 years, dashed grey lines) and (d) the median reduction over three generation lengths (dashed line) and corresponding probabilities for rates of population reduction falling within the IUCN Red List categories.

North Atlantic 2: NOAA CPUE data (1994–2017), Western North Atlantic and Gulf of Mexico, relative abundance (numbers of sharks per 100 hooks and per 1000 hooks).

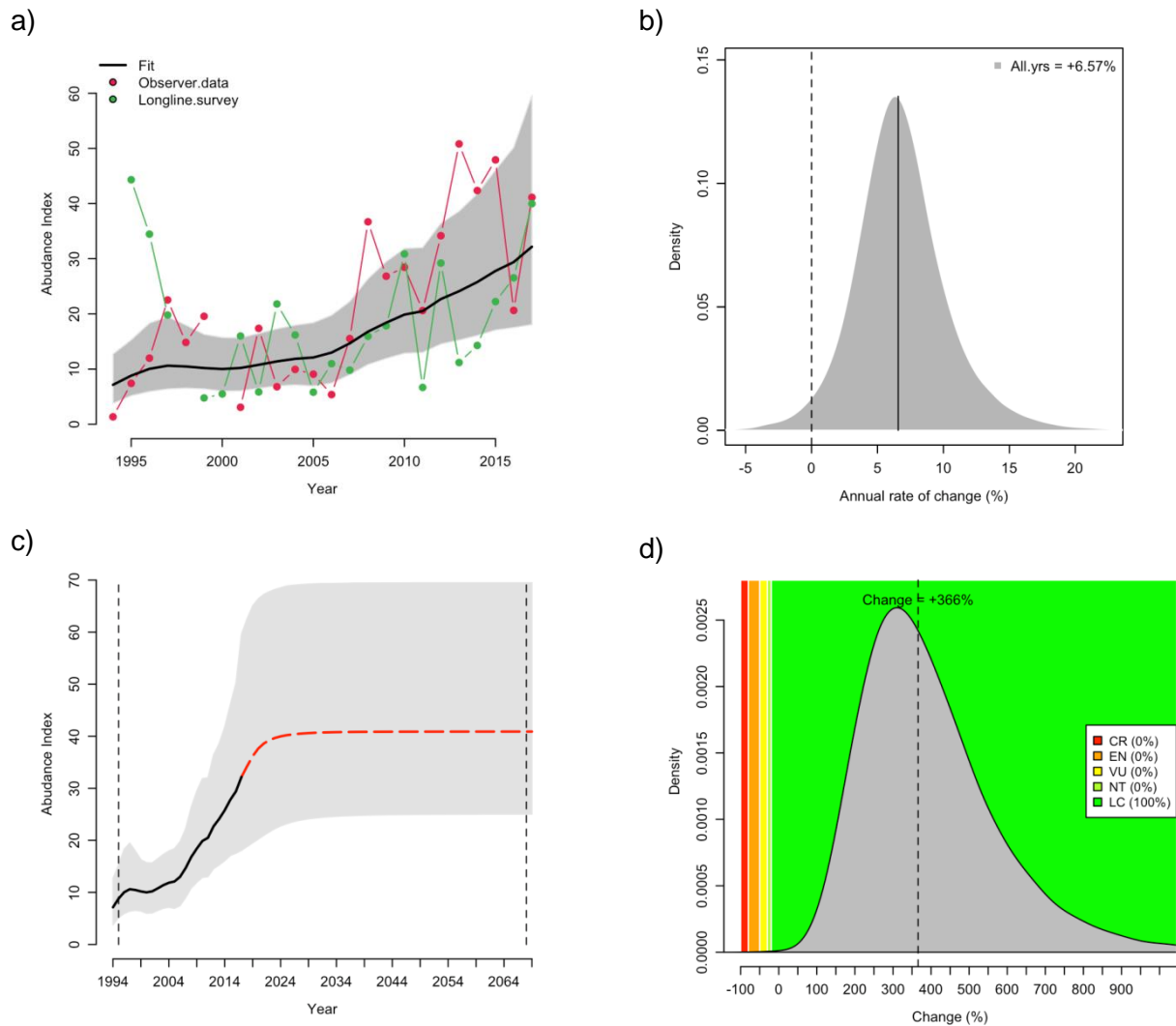


Figure 2. JARA results for Great Hammerhead (*Sphyrna mokarran*) in the north Atlantic showing (a) the JARA fit to the observed time-series, (b) the posterior probability for the percentage annual population change calculated from all the observed data (in black), with the mean (solid lines) shown relative to a stable population (% change = 0, black dashed line), (c) the observed (black line) and predicted (red line) population trajectory over three generations (74.4 years, dashed grey lines) and (d) the median reduction over three generation lengths (dashed line) and corresponding probabilities for rates of population reduction falling within the IUCN Red List categories.

Indian: CPUE (1978–2003), South Africa, gillnet (number per km net year)

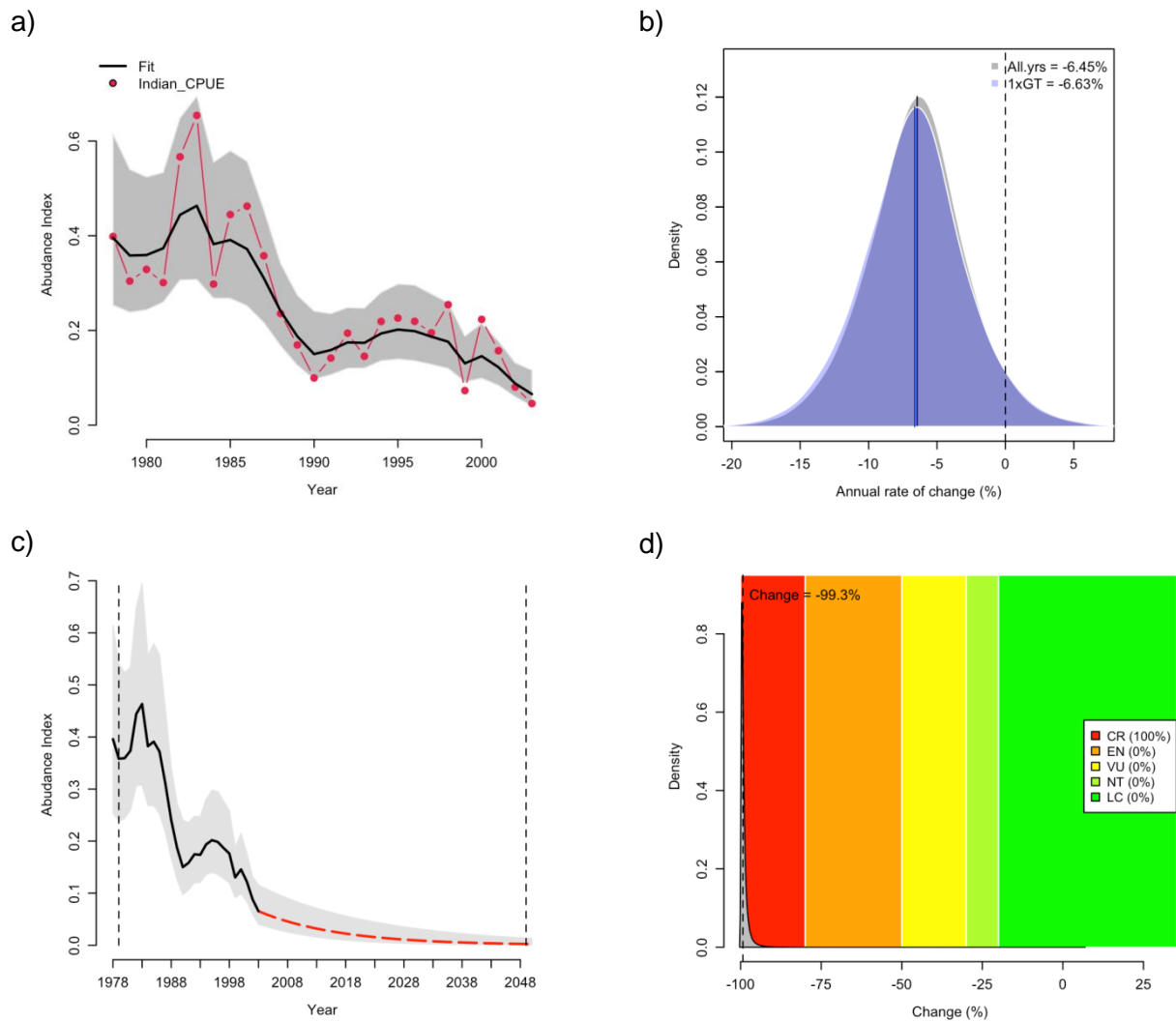


Figure 3. JARA results for Great Hammerhead (*Sphyrna mokarran*) in the Indian Ocean showing (a) the JARA fit to the observed time-series, (b) the posterior probability for the percentage annual population change calculated from all the observed data (in black), with the mean (solid lines) shown relative to a stable population (% change = 0, black dashed line), (c) the observed (black line) and predicted (red line) population trajectory over three generations (71.1 years, dashed grey lines) and (d) the median reduction over three generation lengths (dashed line) and corresponding probabilities for rates of population reduction falling within the IUCN Red List categories.

Global weighted trend 1 (using North Atlantic 1 and Indian

Median (95% CI) change = -62.4% (-99.8–73.0%).

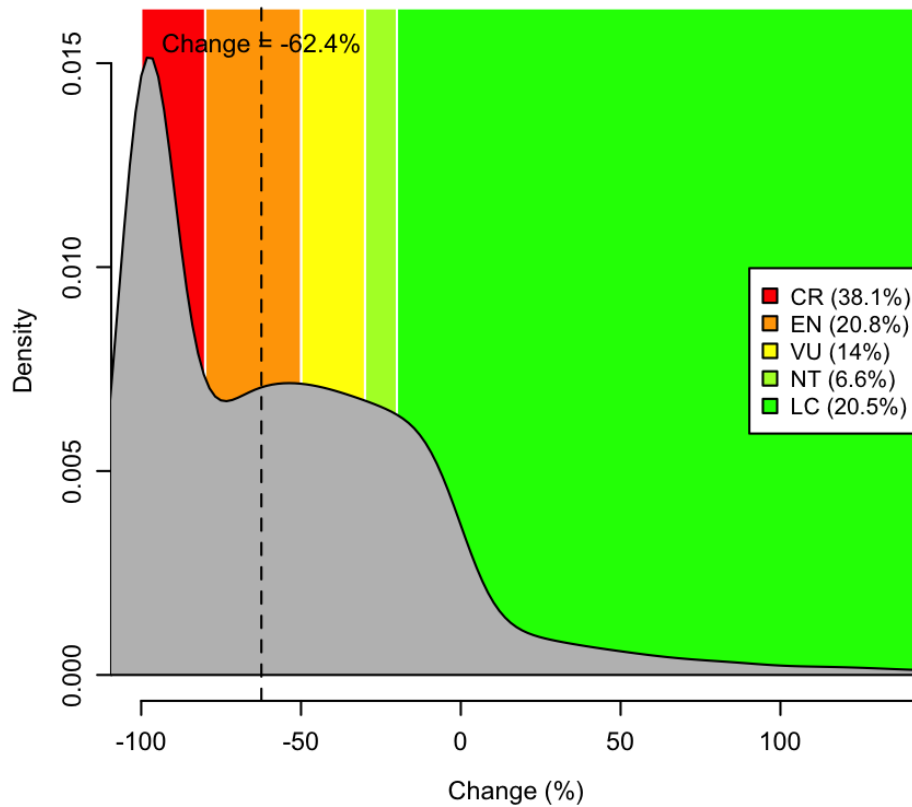


Figure 4. Global weighted trend for *Sphyrna mokarran* based on weighting the regional posterior probabilities for the rates of population reduction over three generations by the relative area of each region as a proportion of the species' global distribution. A uniform distribution $U(-100,0)$ was applied for each region in which the species occurs but no trend data were available.

Global weighted trend 2 (using North Atlantic 2 and Indian):

Median (95% CI) change = -50.9% (-99.8–655.1%).

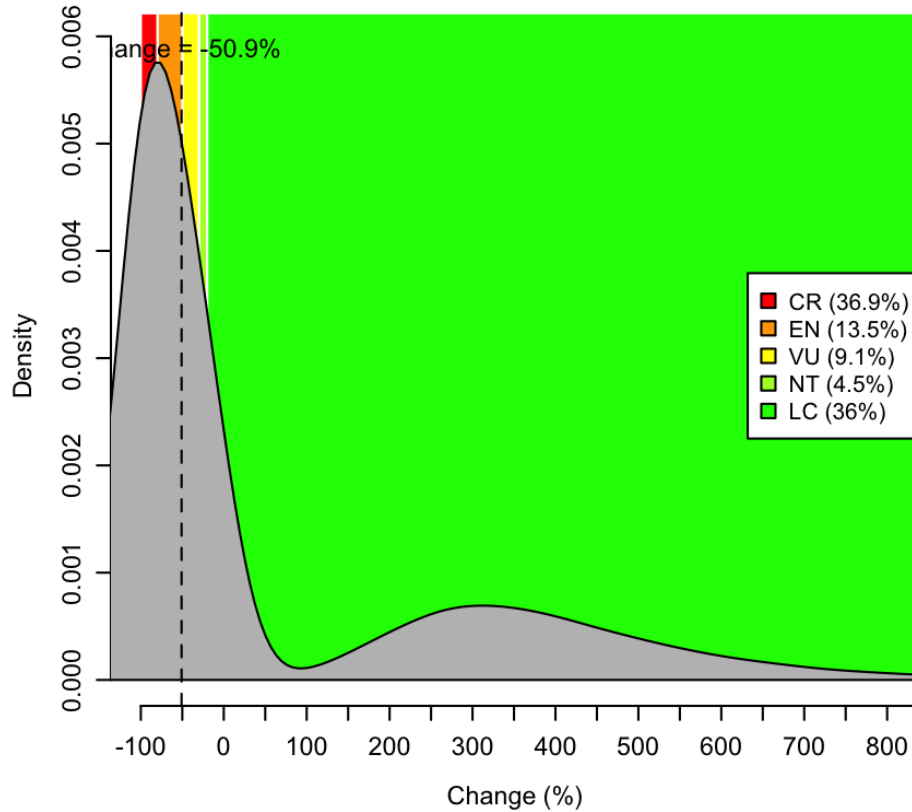


Figure 5. Global weighted trend for *Sphyrna mokarran* based on weighting the regional posterior probabilities for the rates of population reduction over three generations by the relative area of each region as a proportion of the species' global distribution. A uniform distribution $U(-100,0)$ was applied for each region in which the species occurs but no trend data were available.

References

- Chaloupka, M. and Balazs, G. (2007) Using Bayesian state-space modelling to assess the recovery and harvest potential of the Hawaiian green sea turtle stock. *Ecological Modelling* **205**: 93–109.
- Dudley, S.F.J. and Simpfendorfer, C.A. (2006) Population status of 14 shark species caught in the protective gillnets off KwaZulu–Natal beaches, South Africa, 1978–2003. *Marine and Freshwater Research* **57**: 225–240.
- Ebert, D.A., Fowler, S., Compagno, L. and Dando, M. (2013) *Sharks of the World: A fully Illustrated Guide*. Wild Nature Press, Plymouth.
- Froese, R., Demirel, N., Coro, G., Kleisner, K.M. and Winker, H. (2017) Estimating fisheries reference points from catch and resilience. *Fish and Fisheries* **18**: 506–526.
- Geweke, J. (1992) Evaluating the accuracy of sampling-based approaches to the calculation of posterior moments. In: *Bayesian Statistics 4: Proceedings of the Fourth Valencia International Meeting*. (eds J.O. Berger, J.M. Bernardo, A.P. Dawid and A.F.M. Smith). Clarendon Press, Oxford, pp 169–193.
- Jiao, Y., Cortés, E., Andrews, K. and Guo, F. (2011) Poor-data and data-poor species stock assessment using a Bayesian hierarchical approach. *Ecological Applications* **21**: 2691–2708.
- Plummer, M. (2003) *JAGS: A Program for Analysis of Bayesian Graphical Models using Gibbs Sampling*, (Vol. 124).
- Plummer, M., Nicky Best, Cowles, K. and Vines, K. (2006) CODA: Convergence Diagnosis and Output Analysis for MCMC. *R News* **6**: 7–11.
- Su, Y.-S. and Yajima, M. (2012) R2jags: A Package for Running jags from R.
- Winker, H., Carvalho, F. and Kapur, M. (2018) JABBA: Just Another Bayesian Biomass Assessment. *Fisheries Research* **204**: 275–288.